Yu *et al. Biochar* (2024) 6:98
https://doi.org/10.1007/s42773-024-00382-7

Biochar

ORIGINAL RESEARCH

Open Access

Converting plastic-contaminated agricultural residues into fit-for-purpose biochar soil amendment: an initial study

Qiuyu Yu[1,2], Xuhui Zhang[1,2], Tao Gao[3], Xueliu Gong[1,2], Jiarong Wu[1,2], Shuai Tian[1,2], Biao Ma[1], Lujiang Xu[4], Stephen Joseph[1,5], Jufeng Zheng[1,2], Rongjun Bian[1,2*] and Lianqing Li[1,2]

Abstract

Addressing agricultural plastic pollution is vital for ecosystem sustainability. Shifting from traditional waste treatments to a sustainable pathway presents both challenges and opportunities for global plastic management. This study investigated the properties and environmental applications of biochar derived from honeydew melon vines contaminated with plastic hanging ropes, pyrolyzed at temperatures of 300, 500, and 700 °C. The resulting biochars were evaluated for their ability to remove Pb and Cd from aqueous solutions. Additionally, a Chinese cabbage pot experiment was conducted to assess the impact of biochar on Pb and Cd immobilization and plant growth in contaminated soil. Results revealed that the properties of biochar varied with pyrolysis temperature. Specifically, incomplete carbonization of plastic ropes was observed at 300 °C, while biochar produced at 500 °C (BC500) showed a higher yield and contained higher levels of available P and K compared to the biochar produced at 700 °C (BC700). The presence of polycyclic aromatic hydrocarbons (PAHs) in biochars increased with temperature but remained within recommended limits. BC500 exhibited the highest adsorption capacities for Pb and Cd at 127 mg g^{-1} and 36 mg g^{-1}, respectively. Soil amendment with BC500 and BC700 significantly improved soil pH, increased the availability of nutrients and microbial biomass, and effectively immobilized Pb and Cd in the soil. Consequently, the biomass yield of Chinese cabbage was enhanced by 119 % and 86 % under BC500 and BC700, respectively. Moreover, the Pb and Cd content in cabbage decreased by more than 80 % and 29 %, respectively. However, PAHs levels in cabbage leaves increased from 9.2 ng g^{-1} in the control to 20.8 ng g^{-1} and 30.4 ng g^{-1} under BC500 and BC700, respectively, remaining below China's standard for benzo(a)pyrene. This study suggests pyrolyzing plastic-contaminated crop residues at 500 °C is a feasible strategy for waste recycling.

Highlights

- The obtained biochar was nutrient-rich, porous, and low in Pb and Cd.
- The PAHs concentrations in the biochars rose with increasing pyrolysis temperatures.
- Biochar pyrolyzed at 500 °C exhibited the highest adsorption capacity for Pb and Cd.
- Biochars significantly promoted cabbage yield and immobilized soil Pb and Cd.
- Biochars raised Acpy and Nap in cabbage leaves but BaP and total PAHs within safe levels.

[†]Qiuyu Yu and Xuhui Zhang have the same contribution in this study

*Correspondence:
Rongjun Bian
brjun@njau.edu.cn
Full list of author information is available at the end of the article

Keywords Agricultural plastic waste, Crop residues, Biochar, Soil amendment

Graphical Abstract

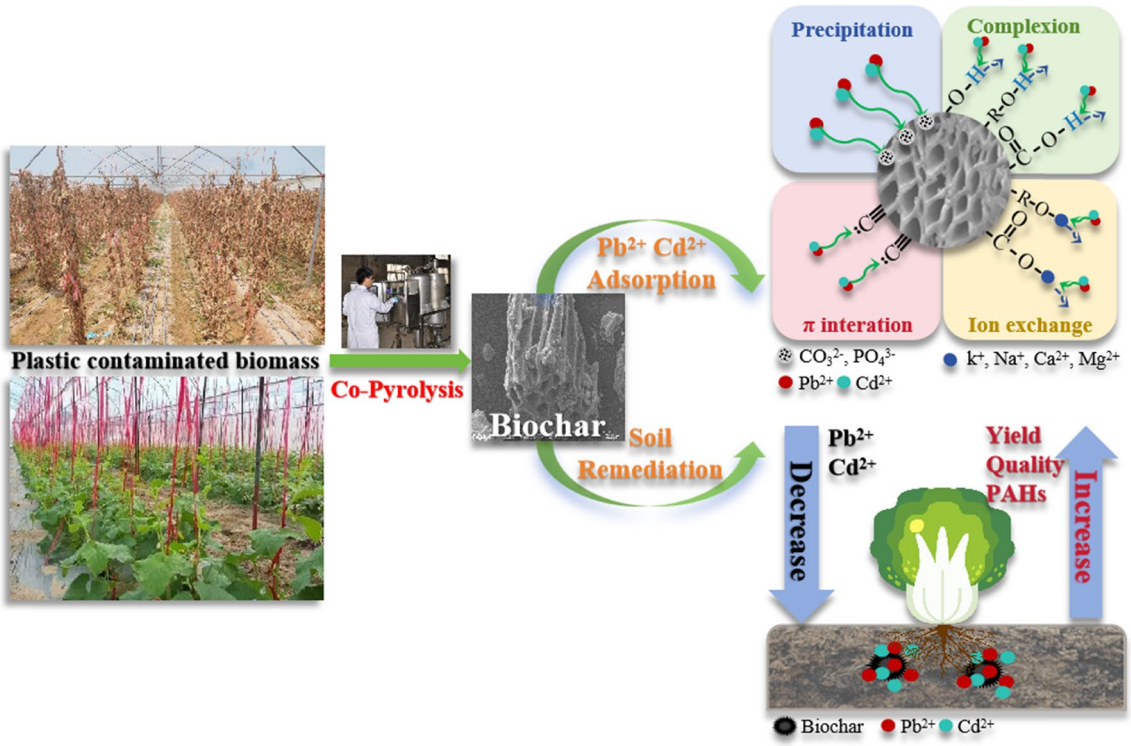

1 Introduction

Plastic pollution has become a critical global issue, pervasively affecting ecosystems from the ocean floor to mountaintops (MacLeod et al. 2021). Plastics are widely utilized in agricultural applications, encompassing coated seeds, controlled-release fertilizers, mulch film and livestock feed bags (Lanorte et al. 2017). The global agricultural plastic use was estimated at 2% of total production (Scarascia Mugnozza et al. 2016). The Food and Agriculture Organization of the United Nations (FAO) reported an annual global consumption of 12.5 million tons of plastics in both plant and animal agriculture (FAO 2022). The utilization of agricultural mulch film in China reached 1.4 million tons in 2017, with an historical accumulated residue of 1.2 million tons (MEPRC 2020). Exposure to the environment leads to the physical weathering of plastic waste, which decomposes into microplastics through heat and ultraviolet radiation (Xu et al. 2020). The increasing content of microplastic in soil has multiple impacts on the physical and chemical properties and microbial characteristics of the soil, resulting in the decline of soil fertility (Tang 2023). Environmental concerns related to plastic additives such as bisphenol A, brominated flame retardants, phthalate esters, and perfluorinated alkyl substances, have attracted global attention (Tang 2023). Global meta-analyses revealed that persistent plastic residues in agricultural fields can significantly reduce crop yields by 3% and adversely affect soil properties and functions (Zhang et al. 2020). Considering the limited and stressed agricultural soils, initiatives are underway to prevent further degradation by enhancing the production and management of plastic-containing agricultural products (Tang 2023).

To address plastic-related agricultural risks, various strategies have been adopted. China's agricultural film rules required users to collect non-biodegradable film waste for recycling before it expires, prohibiting random disposal, burial, or incineration. (Huang 2020). Beside

such collectable film, plastic materials challenging to separate and recycle can lead to more severe environmental issues. For instance, plastic hanging ropes, used extensively in greenhouses to support climbing crops like watermelon and honeydew melon, exemplify this concern (Zhang et al. 2017; Lu and Gao 2019). These ropes enhance space utilization, maximize sunlight exposure, and simplify the harvesting process (Kou et al. 2020). Farmers might improperly dispose of worn-out or damaged plastic ropes, resulting in environmental pollution through actions such as abandoning them in fields, burning, or improper landfilling (Qi et al. 2020). Crop residues often become entangled with plastic ropes, complicating their separation and thus the waste management and recycling processes. The introduction of plastic ropes or other plastics into composting can further contaminate the compost, affecting its quality (Zhang et al. 2023). There is an urgent need to develop strategies to prevent plastic from entering the environment at the source.

Co-pyrolysis technology is considered to be a significant and promising method for converting plastic and biomass waste into value-added products (Wang et al. 2021; Wu et al. 2023). Plastics are polymers with long-chain carbon-based molecules, structurally and elementally akin to biomass macromolecules, primarily consisting of C–C, C-O, and C-H bonds (Li et al. 2023). The structural similarities between plastics and biomass resulted in similar chemical bond activating chemical bonds and catalyzing conversion properties. Pyrolysis thermally decomposes plastic into hydrocarbons for liquid fuels without the need for extensive pretreatment or sorting (Dai et al. 2024; Li et al. 2023). Khan et al. (2005) suggested that biochar and low-molecular-weight tar produced during co-pyrolysis were rich in free radicals that promoted the plastic decomposition.

Co-pyrolysis of biomass and plastics, especially within the medium to high-temperature range, benefited from a synergistic effect that enhances thermal decomposition efficiency and improves biochar yield and quality (Wu et al. 2023). This efficiency was partly due to co-pyrolysis reducing the feedstock's thermal activation energy (Rathnayake et al. 2021). The synergistic effect arose from the secondary free radicals generated during co-pyrolysis, which catalyzed inter-molecular hydrogen transfer, monomer formation, ethylene isomerization, and molecular polymerization (Zhou et al. 2014). Co-pyrolysis of rice straw with oxygen-rich polyethylene terephthalate (PET) resulted biochar with an increasesd surface area, improved surface functional groups, and enhanced cation exchange capacity compared to biomass-only pyrolysis (Oh and Seo 2019; Rodriguez et al. 2021). This characteristics lead to superior adsorption properties, which are beneficial for soil enhancement (Rodriguez et al. 2021). In a co-pyrolysis system, the inclusion of plastics not only improved biochar properties but also markedly increased the yield and quality of bio-oil and pyrolysis gas (Liu et al. 2020; Xie et al. 2023). Studies indicated that co-pyrolysis substantially enhanced the yields of H_2, CO, and C_2H_4 when the biomass-to-plastics mass ratio was below 80%, and the formation of C_3H_6 was notably boosted when this ratio droped below 60% (Kai et al. 2019).

The distribution of pyrolysis products in co-pyrolysis is influenced by various factors. Temperature, reaction time, biomass components, and catalyst type (Sebestyén et al. 2017) all affected the yields and composition of pyrolysis products. Pyrolysis temperature is a key factor, significantly affecting the quantity, variety, and chemical composition of the products (Wu et al. 2023), impacting the properties of bio-oil, biochar, and syngas. Reaction time primarily affected the yields of pyrolysis products (Sun et al. 2020). Additionally, the interaction between biomass and plastic in co-pyrolysis can result in either synergistic or antagonistic effects on the formation of organic pollutant, which also depends on type of feedstock and pyrolysis conditions (Hassan et al. 2020; Wu et al. 2023). The co-pyrolysis of corn stover and high-density polyethylene reached its maximum monocyclic aromatic yield at 550 °C, as reported by Lin et al. (2023). However, elevated temperatures trigger the formation of polycyclic aromatic hydrocarbons (PAHs) and concurrently decrease the presence of monocyclic aromatic, attributed to undesirable aromatic polymerization reactions (He et al. 2021b). Nevertheless, co-pyrolysis of rapeseed stalk with chlorine-rich polyvinyl chloride (PVC) can inhibit PAHs formation, unaffected by temperature (Wu et al. 2023). Currently, although the synergistic effects of co-pyrolysis have been recognized, there is a notable gap in research on the safety of biochar from co-pyrolysis for plastic-contaminated crop residues and its environmental and soil amendment potential. This indicates an urgent requirement for further research.

In this study, honeydew melon vines, entwined with plastic ropes, were sourced from Ledong County, where the melon cultivation area reached 4,500 hectares in 2021, resulting in 140,000 tons of vine waste in three seasons per year. Hanging ropes are essential for ensuring yield and quality in cultivation. However, the polypropylene ropes used pose environmental risks due to the difficulty of separating them from vines and the challenges associated with traditional disposal methods. Traditional waste disposal methods, such as landfilling and incineration, which are recognized to have negative ecological impacts, are no longer permitted. The samples were subjected to pyrolysis across a range of temperatures, followed by a comprehensive characterization of the biochar produced. The adsorption capacity of biochars for

Pb^{2+} and Cd^{2+} ions in aqueous solutions were evaluated, with these heavy metals selected for their significant bioavailability and potential health impacts within the food chain (Qin et al. 2021; Yao et al. 2021). Pot experiments with Cd^{2+} and Pb^{2+} contaminated soil were conducted to evaluate the biochar's efficacy and safety for soil remediation. The objective of this study was to contribute to the understanding of co-pyrolysis technologies for managing plastic-contaminated crop residues and to explore their transformation into value-added products for agriculture production.

2 Materials and methods

2.1 Biochar production

The raw wastes were removed from the field and naturally air-dried after harvest. The honeydew melon vines and the plastic ropes were weighed separately and the plastic rope content in the mixture was 8%. Subsequently, vine wastes blended with hanging ropes were evenly mixed after being crushed with a shredder. For pyrolysis, 1 kg of chopped feedstock was fed into a bench-scale pyrolyzer (SSBP-5000A, Huadian Environmental Machinery Co., Ltd., Jiangsu, China) (Fig. S2). The pyrolysis temperatures were set at 300 °C, 500 °C, and 700 °C, with a heating rate of 10 °C min^{-1}, maintained for 1 h at the highest temperature before naturally cooling down to room temperature. The obtained biochar was named BC300, BC500, and BC700, respectively, and the yields were recorded. It should be noted that due to incomplete pyrolysis of raw material in the feedstock at 300 °C, further investigation was not conducted on BC300. BC500 and BC700 were screened with 20-mesh and 100-mesh nylon screens, respectively, and stored in sealed bags for later use.

2.2 Characterization of biochar

The biochar yield was calculated as the ratio of the weight of biochar obtained after pyrolysis to the weight of the raw materials. The pH and electrical conductivity (EC) were determined by mixing biochar with ultrapure water at a ratio of 1: 20, using a pH meter (PHB-5 portable pH meter of Shanghai Leici) and a conductivity meter (Shanghai Rex DDS-11A, China). The organic carbon content was assessed using the external heating method with K_2CrO_7-$FeSO_4$. The contents of carbon **(C)**, hydrogen (H), oxygen (O), nitrogen (N) and sulfur (S) in biochar samples were determined by an element analyzer (Elementar Unicube, Germany). After digesting the biochar sample with H_2SO_4-H_2O_2, the total potassium content was measured using a flame spectrophotometer (FP6410, Shanghai analyzer electricity co., ltd), and the total phosphorus content was determined using the method of Molybdenum Antimony Anti-Colorimetric (A360 spectrophotometer, Beijing Puxi General Instrument Co., Ltd.). Utilizing a 2% formic acid solution for extraction, the vanadium molybdenum yellow colorimetric method was employed to develop color, and a spectrophotometer was utilized to quantify the available phosphorus content. The content of available potassium was determined using a flame spectrophotometer following extraction with a 1 M neutral NH_4OAc solution. The biochar sample (0.5 g) was digested with mixed acid solution of 85% HNO_3 and 15% $HClO_4$ for total concentrations of metals including Fe, Mn, Cu, Zn, Pb, and Cd inductively coupled plasma mass spectrometry (ICP-MS, Thermo Fisher Scientifc, Inc., iCAPQ, USA). The specific surface area of biochar sample was determined using the Brunauer–Emmett–Teller (BET), which was derived from N_2 adsorption isotherms at 77.3 K with a Micromeritics ASAP 2460 Version 3.01 analyzer. Surface microscopic topography was characterized by scanning electron microscopy and energy dispersive X-ray spectroscopy (SEM–EDS, Hitachi Regulus 8100). Surface functional groups were identified through Fourier transform infrared spectroscopy (FT-IR; Thermo Scientific Nicolet iS20). Mineral characterization was conducted using an X-ray diffractometer (XRD; Rigaku MiniFlex600). The concentrations of the 16 monomers of USEPA priority pollutant PAHs in biochar samples were determined using a protocol provided by the International Biochar Initiative (IBI). PAHs contents in biochar were determined through thermal extraction and gas chromatography-mass spectrometry (GCMS, Shimadzu-QP2010, SESY-001) with detailed methodology provided in the supplementary materials. The toxic equivalent (TEQ) quantifies the carcinogenic potential of PAHs, calculated using the following formula:

$$TEQ_i = PAH_i \cdot TEF_i \tag{1}$$

$$TEQ = \sum \left(TEQ_i\right) \tag{2}$$

where TEF_i represents the toxic equivalent factor for an individual PAH monomer, TEQ_i is the toxic equivalent factor for a PAH monomer, PAH_i denotes the toxic equivalent factor for a PAH monomer, and TEQ is the cumulative toxic equivalent of multiple PAH monomers. The determination of TEF_i follows the methodology outlined in the IBI (International Biochar Initiative 2015).

The biochar samples were fortified with an internal standard solution, and the dioxin content was determined by gas chromatography-mass spectrometer (Shimadzu GCMS-QP2010 SESY-001) following extraction, purification, and concentration, in accordance with the HJ77.3–2008 protocol. Further details are provided in the supplementary materials.

2.3 Adsorption experiment

In the adsorption experiment, solutions for adsorption were prepared using cadmium nitrate tetrahydrate ($Cd(NO_3)_2{\cdot}4H_2O$) or lead nitrate ($Pb(NO_3)_2$), with 0.01 M $NaNO_3$ as the background electrolyte. The initial pH was adjusted to 5.5, and biochar dosage was 0.05 g in a 25 ml adsorption solution. Pb^{2+} or Cd^{2+} concentration was quantified in the solution using a flame atomic absorption spectrophotometer (AAS, A3, China Purity Company). The adsorption capacity was calculated using the formula:

$$Q = (C_1 - C_2)V/m. \tag{3}$$

where Q (mg g^{-1}) is the calculated adsorption amount, C_1 (mg L^{-1}) is the initial concentration of Cd^{2+} or Pb^{2+}, C_2 (mg L^{-1}) is the concentration of residual Cd^{2+} or Pb^{2+} in the adsorption solution determined after the adsorption reaction, V (mL) is the volume of the adsorption liquid, and m (g) is the dosage of biochar.

2.3.1 Adsorption kinetics

The initial pH of the adsorption solution was adjusted as 5.5, with Pb^{2+} concentration at 600 mg L^{-1} and Cd^{2+} concentration at 150 mg L^{-1}. The biochar sample was thoroughly mixed with the solution and shaken for 5 min to 24 h. After various reaction times, the adsorbed solution was filtered, and the concentration of Cd^{2+} or Pb^{2+} in the filtrate was determined. The pseudo-first-order kinetic model and quasi-second-order kinetic model were utilized to fit the adsorption kinetic curve.

$$q_t = q_e\left(1 - e^{-k_1 t}\right) \tag{4}$$

$$q_t = (k_2 q_e^2 t)/(1 + k_2 q_e t)t. \tag{5}$$

$$h = k_2 q_e^2 \tag{6}$$

where K_1 (h^{-1}) and K_2 (g mg^{-1} h^{-1}) are adsorption rate constants for pseudo-first-order kinetic model and pseudo-second-order model, t (h) is the time of adsorption, q_e (mg g^{-1}) is the equilibrium adsorption capacity, and q_t (mg g^{-1}) is the instantaneous adsorption amount at a special reaction time (t). In Formula (6), h (mg g^{-1} h^{-1}) is a derivative parameter calculated from pseudo-second-order adsorption kinetics, offering an approximation of the absolute reaction rate during the initial adsorption stages.

2.3.2 Adsorption isotherm

The Pb^{2+} adsorption solutions spanned concentrations from 2 mg L^{-1} to 1300 mg L^{-1}, and the Cd^{2+} adsorption solutions ranged from 2 mg L^{-1} to 150 mg L^{-1}. The initial solutions were adjusted to a pH of 5.5 and agitated for 24 h at 300 rpm to achieve equilibrium. The isothermal adsorption was modeled using both Langmuir and Freundlich equations.

$$q_e = (bC_eQ_{max})/1 + bC_e. \tag{7}$$

$$q_e = K_f C_e{}^{1/n} \tag{8}$$

where Q_{max} (mg g^{-1}) is the maximum adsorption capacity calculated by Langmuir model, and B (L mg^{-1}) is Langmuir model constant. In formula (8), K_f is the Freundlich model constant, and 1/n can reflect the adsorption strength. q_e (mg g^{-1}) is the adsorption amount at equilibrium, and C_e (mg L^{-1}) is the concentration of Pb^{2+} and Cd^{2+} in the equilibrium solution.

2.3.3 Effect of initial pH value of solution

The initial pH values of the Pb^{2+} (600 mg L^{-1}) and Cd^{2+} (150 mg L^{-1}) solutions were systematically adjusted to 1.5, 2.5, 3.5, 4.5, 5.5, and 6.5. Biochar samples were weighed into individual plastic tubes, and the mixtures of adsorbent and solution were shaken at 180 rpm for 24 h at 25 °C to reach equilibrium. The equilibrium pH value of the solution was measured with a pH meter after standing. The suspension was filtered and analyzed using atomic absorption spectroscopy.

2.3.4 Fractions of adsorbed Pb/Cd on biochar

The biochar samples post-Cd^{2+} or Pb^{2+} adsorption were collected and dried at 60 °C in an oven for 48 h. Mineralogical and functional group alterations were evaluated using FT-IR, XRD, and SEM–EDS analyses. The characterization of adsorbed Cd^{2+} and Pb^{2+} fractions on the biochar surface was conducted through a simplified sequential extraction method (Supplementary materials) (Lian et al. 2020).

2.4 Pot experiment

A pot experiment was conducted in the greenhouse of Nanjing Agricultural University to assess the potential influence of biochar on plant growth and its effect on soil Cd and Pb immobilization. A topsoil (0–15 cm) sample was collected from a paddy field contaminated with heavy metals due to historical industrial emissions in Tongling County, Anhui Province, China. The collected soil sample was air-dried and ground to pass through a 2 mm sieve to ensure homogeneity prior to experiment. The basic properties of the homogenized topsoil prior to the experiment were as follows: the soil organic carbon (SOC) content was 28.50 g kg^{-1}, and the concentrations of soil total nitrogen (N), phosphorus (P), potassium (K) were

1.70 g kg^{-1}, 0.31 g kg^{-1} and 11.95 g kg^{-1}, respectively. The available P and K of in the topsoil were 25.19 mg kg^{-1} and 110.33 mg kg^{-1}, respectively. Additionally, the soil samples contained 1.79 mg kg^{-1} of Cd, 180 mg kg^{-1} of Pb, 20.77 mg kg^{-1} of Cu, and 142.57 mg kg^{-1} of Zn. with a pH (H_2O) value of 5.37. Three treatments included a control (CK) without soil amendment and two treatments involving the addition of BC500 and BC700. In a plastic pot with 20 cm in height and 25 cm in diameter, 1.98 kg of homogenized soil and 20 g of biochar were added and thoroughly mixed for each treatment.

This study employed Chinese cabbage (*Brassica chinensis* L.), a commonly consumed vegetable, as a model to investigate the safety implications of biochar and its impact on the immobilization of soil Pb and Cd. The experimental procedure involved the application of 0.65 g pot^{-1} urea, 0.44 g pot^{-1} $NH_4H_2PO_4$, and 0.74 g pot^{-1} K_2SO_4, with the soil moisture content being maintained at 70% of the field water holding capacity for 5 days before sowing 10 Chinese cabbage seeds in each pot. Following the appearance of the third true leaf, four comparable seedlings were randomly selected and grown in the greenhouse until harvest. Each treatment was replicated three times, and all pots were arranged in a random permutation. Cabbage seeds were sown on August 13, 2023, and harvested on September 25, 2023. During harvesting, the edible parts of the cabbage and roots were sampled and weighed to determine the fresh biomass yield. After washing with deionized water, the fresh cabbage was crushed and homogenized into small pieces. One part of the crushed fresh sample was immediately used for quality analysis, and the other part was oven-dried at 105 ℃ for 30 min and then at 60 °C for 24 h. The dried samples were then ground and stored in sealed bags. For soil sampling, 150 g of fresh soil was randomly collected during soil homogenization after harvest. All soil samples were air dried and passed through a 0.85 mm and 0.125 mm sieve sequentially before chemical analysis. In addition, another 200 g soil sample was obtained from each pot after harvest for microbial biomass analysis.

The soil samples were characterized following the methodology outlined by Bao (Bao 2000). Soil pH was determined in distilled water with a soil-to-water ratio of 1:2.5 (m/v). Soil organic matter (SOM) content was assessed through $K_2Cr_2O_7$ oxidation. Total concentrations of Cd and Pb were determined by digesting 0.2 g of air-dried soil with 4 ml HCl and 1 ml HNO_3. For evaluating the available fractions of soil Cd and Pb, 5 g of air-dried soil was extracted with a solution containing 0.01 M $CaCl_2$. The concentrations of Cd and Pb in both the digested and extracted solutions were quantified using ICP-MS (Thermo Fisher Scientifc, Inc., iCAPQ, USA). 12.5 g of fresh soil samples were fumigated in a vacuum dryer with or without chloroform for 24 h, and then the concentrations of SMBC and SMBN were determined using a carbon and nitrogen analyzer (Germany jena multi N/C3100). Concentrations of soluble sugar in the edible parts of the cabbage were determined by anthone colorimetric assay at 620 nm using a spectrophotometer (UV-3600i Plus, Shimadzu Co., Tokyo, Japan).

The cabbage's total nitrogen (N), phosphorus (P), and potassium (K) contents were determined according to the procedures described in Bao (2000). Specifically, 0.15 g of dried biomass was weighed, digested with 5 mL H_2SO_4-H_2O_2, and analyzed for total N using an automatic Kjeldahl nitrogen analyzer (KDN-1, Leici Co., Shanghai, China). Total P content was quantified using the vanadium-molybdenum-yellow photometric method, and total K content was measured with a flame photometer (FP6410, Shanghai analyzer electricity co., ltd). For Cd and Pb measurements in the cabbage's edible parts and roots, 0.1 g of dried biomass was digested with an HNO_3-$HClO_4$ solution (4:1, v:v) and analyzed via ICP-MS (Thermo Fisher Scientifc, Inc., iCAPQ, USA).

The PAHs in cabbage were extracted by solvent, saponified by potassium hydroxide ethanol solvent, purified by solid phase extraction column, concentrated and determined by gas chromatography-mass spectrometry (PerkinElmer Clarus 580), and quantified by isotope internal standard method (GB5009.265–2021) and details are presented in the supplementary materials.

3 Results and discussion

3.1 Properties of biochar

3.1.1 Physicochemical properties of biochar

The rise in pyrolysis temperature from 500 ℃ to 700 ℃ resulted in a decrease in biochar yield, from 50.38% to 43.57% (Table 1). This reduction is attributed to elevated temperatures causing the breakdown of organic compounds into gaseous molecules such as carbon monoxide, carbon dioxide, hydrogen, and methane, released from the matrix. Additionally, the decomposition of lignin and cellulose contributed to the decline in yield (Yang et al. 2019). Surface acidic functional groups on biochar gradually decomposed, while alkaline inorganic substances accumulated at higher pyrolysis temperatures (Zhang et al. 2015), leading to an increase in biochar pH from 11.12 to 11.88 (Table 1). Elemental analysis highlighted C and O as the primary biochar elements. The pyrolysis temperature did not significantly influence the content of C, H, O, and S. However, a significant decrease in N content was observed, attributed to the volatilization of nitrogen oxides (NO_x) (Shi et al. 2023). The study demonstrated a reduction in the H/C and O/C ratios of biochar from 0.08 and 0.49 to 0.07 and 0.46, respectively, with the temperature rising from 500 ℃ to 700 ℃ (Table 1).

Table 1 The physiochemical properties of biochars

	BC500	BC700	IBI[a]	EBC[b]-AgroOrganic	EBC[b]-Agro
Yield (%)	50.4 ± 5.6a	43.6 ± 3.3a			
C (%)	38.63 ± 0.08a	37.17 ± 0.08b			
H (%)	3.03 ± 0.07a	2.59 ± 0.07b			
O (%)	19.01 ± 0.07a	17.27 ± 0.07b			
N (%)	3.02 ± 0.04a	2.50 ± 0.06b			
S (%)	0.78 ± 0.06a	0.82 ± 0.07a			
Organic carbon (C_{org}) (%)	32.67 ± 3.52b	36.34 ± 1.23a			
H/C_{org}	0.09 ± 0.00a	0.07 ± 0.00b	0.7	0.7	0.7
O/C_{org}	0.58 ± 0.00a	0.48 ± 0.00b			
pH	11.12 ± 0.10a	11.88 ± 0.60a			
Total P (g kg^{-1})	6.55 ± 1.67b	8.35 ± 0.53a			
Total K (g kg^{-1})	55.81 ± 2.73a	53.84 ± 2.90a			
Total Fe (g kg^{-1})	3.47 ± 0.18b	5.14 ± 1.05a			
Total Mn (g kg^{-1})	0.57 ± 0.02a	0.43 ± 0.02b			
Total Zn (mg kg^{-1})	107.99 ± 1.78a	93.52 ± 2.43b	416–7400	200	400
Total Cu (mg kg^{-1})	24.54 ± 0.55a	20.75 ± 0.72b	143–6000	70	100
Total Pb (mg kg^{-1})	2.49 ± 0.10a	2.26 ± 0.08a	121–300	45	120
Total Cd (mg kg^{-1})	0.61 ± 0.02a	0.51 ± 0.01b	1.4–39	0.7	1.5
Available P (g kg^{-1})	3.69 ± 0.08a	2.82 ± 0.02b			
Available K (g kg^{-1})	51.39 ± 0.89a	39.22 ± 1.32b			
Specific surface area (m^2 g^{-1})	4.12	7.46			
Average pore size (nm)	15.59	19.66			
Total pore volume (cm^3 g^{-1})	0.016	0.037			
PAHs (mg kg^{-1})[c]	10.77 ± 0.10b	69.66 ± 0.94a	6–300	6.0 ± 2.4	6.0 ± 2.4
TEQ of PAHs (mg kg^{-1})	0.19 ± 0.01b	2.98 ± 0.03a	3		
PCDD/FS (ngTEQ kg^{-1})	2.00 ± 0.10b	3.00 ± 0.40a	17	20	20

Values are presented as mean ± standard deviation (n = 3). Different lowercase letters within a single column indicate a significant difference between the treatments at $p < 0.05$. BC500 and BC700, biochar produced at 500 °C and 700 °C, respectively

[a] International Biochar Initiative (IBI) certification program requirements, Version 2.1 of November 23, 2015

[b] European Biochar Certificate (EBC) guidelines for a sustainable production of biochar, Version 10.3E of 5th April 2023

[c] The concentrations of 16 PAH monomers (mg·kg^{-1}) are provided in Table S1

With increasing temperature, the total P content in biochar rose, while available P decreased due to stabilization in insoluble forms, such as the formation of $Ca_3(PO_4)_2$ (Shi et al. 2023). BC500 exhibited higher available potassium than BC700, attributed to the volatilization process, wherein KCl or KOH entered the gas phase as K^+ with rising temperature (Shi et al. 2023). The N content in both BC500 and BC700 exceeded 2.5%, while the total P and K content reached 60 g kg^{-1} (Table 1), surpassing the levels typically found in biochars from crop residues and manure, and meeting or exceeding China's standards for organic fertilizer (Shi et al. 2023; Zhao et al. 2013). This indicates the significant role of biochar derived from honeydew melon vines in enhancing soil fertility through the supplementation of essential mineral nutrients (Aziz et al. 2023; Wang et al. 2018c).

The concentrations of heavy metals and organic pollutants in biochar were compared with the regulations specified by the European Biochar Certificate (EBC 2023) and the International Biochar Initiative Guide (IBI 2015). For soil amendment purposes, the EBC standard for biochar intended for use in organic agriculture is the most stringent, specifying maximum permissible concentrations of Pb, Cd, Zn, and Cu at 45 mg kg^{-1}, 0.7 mg kg^{-1}, 200 mg kg^{-1}, and 70 mg kg^{-1}, respectively. It is evident that the levels of Pb, Cd, Cu, and Zn in biochar fall below the prescribed values (Table 1). Furthermore, the concentrations of PAHs in biochar exceed the specified values of the EBC (6–300 mg kg^{-1}) but remain within the maximum threshold set by the IBI (6.0 ± 2.4 mg kg^{-1}). Notably, the PAHs content of BC500 is significantly lower, being only 15.46% of that in BC700 (Table 1). The observed

significant increase in PAHs may be attributed to demethylation reactions, a phenomenon consistent with the findings of Zhou et al. (2016). In their study, they noted the formation of 2–4-ring PAHs during the pyrolysis of PVC as the temperature increased from 500 °C to 900 °C. Moreover, Mohseni-Bandpei et al. (2019) investigated the impact of pyrolysis temperature on PAHs production during the pyrolysis of low-density polyethylene and reported elevated formation of benzene, naphthalene, and methylnaphthalene with an increase in temperature from 500 to 700 °C. The increase in PAHs with rising temperature was attributed to the promotion of secondary tar reactions. On the contrary, for biomass waste products such as crop residues, wood, paper sludge, the content of PAHs decreases with the increasing pyrolysis temperature (Hale et al. 2012; Wang et al. 2017). However, even in the case of pure biomass derived biochars, the concentration of PAHs and the associated environmental risks still merit attention and careful consideration. Wang et al. (2018a) analyzed both commercial biochar and laboratory-prepared biochar, finding that the concentration of PAHs ranged from 0.5 to 27 mg kg^{-1}, which could be lead to a potential risk to human health as soil amendment. In this study, the total content of monomers with low toxic equivalency factor (TEF = 0.001) values, including naphthalene, acenaphthylene, acenaphthene, flfluorene, phenanthrene, fluoranthene, and pyrene, was notably high (88% for BC500, 75% for BC700). Conversely, those with high TEF values (TEF = 1), such as benzoapyrene and dibenzo(a,h)anthracene, were minimally detected, accounting for only 1% in BC500 and 3% in BC700 (Table S1). Buss et al. (2022) also indicated that naphthalene is the least toxic of the 16 US EPA-listed PAHs but comprises the highest proportion of PAHs in biochar. Consequently, the TEQ range of PAHs for BC500 and BC700 was 0.19 to 2.98, respectively, staying below the safety guidance limit value of 3 established by the IBI (Table 1). Hence, the biochars obtained in this study appeared to pose limited safety risks. The formation of PAHs is predominantly influenced by pyrolysis conditions, including residence time, pyrolysis temperature, carrier gas flow, and plastic content. Previous studies have indicated that factors such as slow pyrolysis, extended residence time, lower moisture content in the feedstock, and increased flow of N_2 tend to lead to a reduced yield of PAHs in biochar (Wang et al. 2017). Buss et al. (2022) discovered that the condensation of pyrolysis vapors in the cool zones of the post-pyrolysis area, rather than the pyrolysis process itself, primarily induces the production of PAHs. Therefore, biochars from high-tech, continuous pyrolysis reactors where volatiles can freely escape and are unlikely to condense, should be recommended for further investigations. This recommendation is in contrast to biochars from traditional kilns or muffle furnace setups that do not allow for the release of pyrolysis volatiles. In addition, the levels of polychlorinated dibenzo-p-dioxins/furans (PCDD/Fs) were found to be well within the guidelines recommended for biochar soil amendment by IBI (17 ngTEQ kg^{-1}) and EBC (20 ngTEQ kg^{-1}) (Table 1). In fact, in addition to the generation of biochar in the pyrolysis process of biomass with plastics, pyrolysis gas will also be generated, and the determination of pollutants should be carried out for pyrolysis gas in the future to further ensure the safety of pyrolysis products.

3.1.2 Surface structure of biochar

The FT-IR analysis of BC500 and BC700 showed comparable functional group patterns (Fig. 1). BC700 exhibited slightly stronger peak intensity, while BC500 demonstrated a broader band width. The observed peak at 3405–3854 cm^{-1}, corresponding to stretching and shrinking vibrations of -OH, indicates a higher content of phenolic or alcoholic hydroxyl groups in BC500 (Ma et al. 2017). The peak at 1622–1632 cm^{-1} corresponds to C=C or benzene ring skeleton tensile vibration, showing an increase with pyrolysis temperature, which indicates enhanced aromaticity, consistent with elemental analysis results (Ma et al. 2019; Huang et al. 2023). The peak at 1431–1438 cm^{-1} is attributed to symmetric stretching vibration of carboxyl salt (–COO) (Parikh et al. 2014). Additionally, peaks at 2922 cm^{-1}, 857 cm^{-1}, and 408–607 cm^{-1} correspond to C–H, C–C, and Si–O/Al-O vibrations, respectively, while the 1100 cm^{-1} peak indicates the stretching vibration of C–O–C (ether or phenol) (Buema et al. 2021; Liao et al. 2022). The predominant mineral phases observed in the biochar samples were KCl, with a secondary presence of NaCl and $CaCO_3$ evident at 2θ peaks of 28.36°, 31.78°, and 29.58°, respectively (Fig. 2).

The SEM images clearly demonstrated the influence of pyrolysis temperature on the surface morphology and pore structure of biochar. In Fig. 3, BC500 exhibits a distinct pore structure. However, as the temperature increased, the skeleton structure of the biochar was compromised, leading to the collapse of the pore structure due to its increased brittleness. Consequently, the overall pore count of BC700 decreased, and the pores became large. This change potentially contributes to the increased specific surface area of BC700 (Table 1). EDS (Fig. S3) results revealed that the surface elements of biochar predominantly composed of C and O, with trace minerals such as Cl, K, Na, and Ca, consistent with the results in Table 1 and XRD.

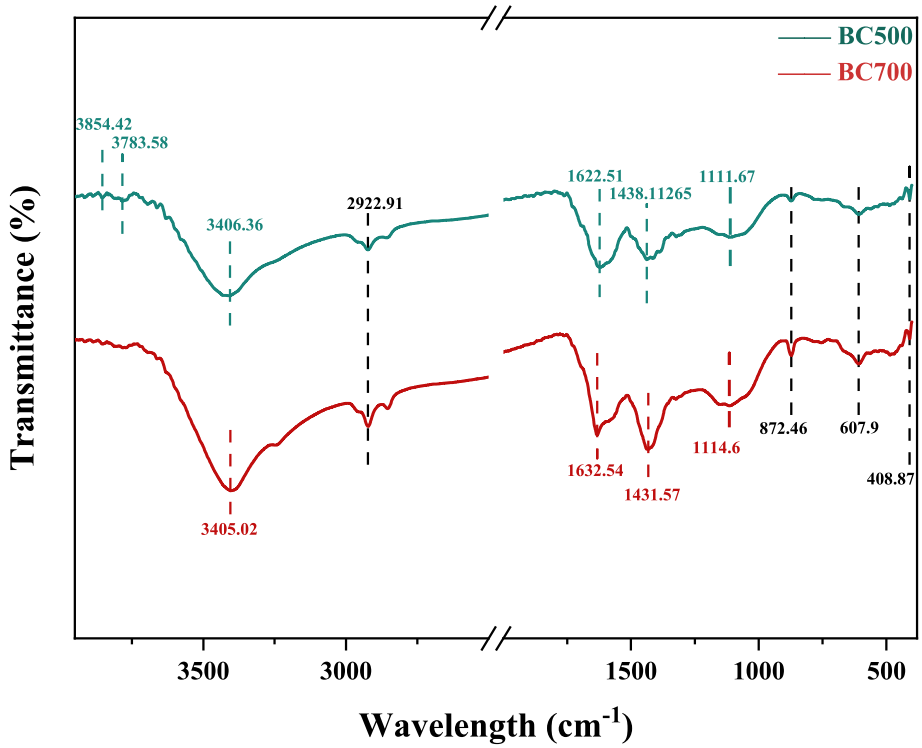

Fig. 1 FT-IR spectra for the biochar samples of BC500 and BC700. BC500 and BC700, biochar samples produced at 500 °C and 700 °C, respectively

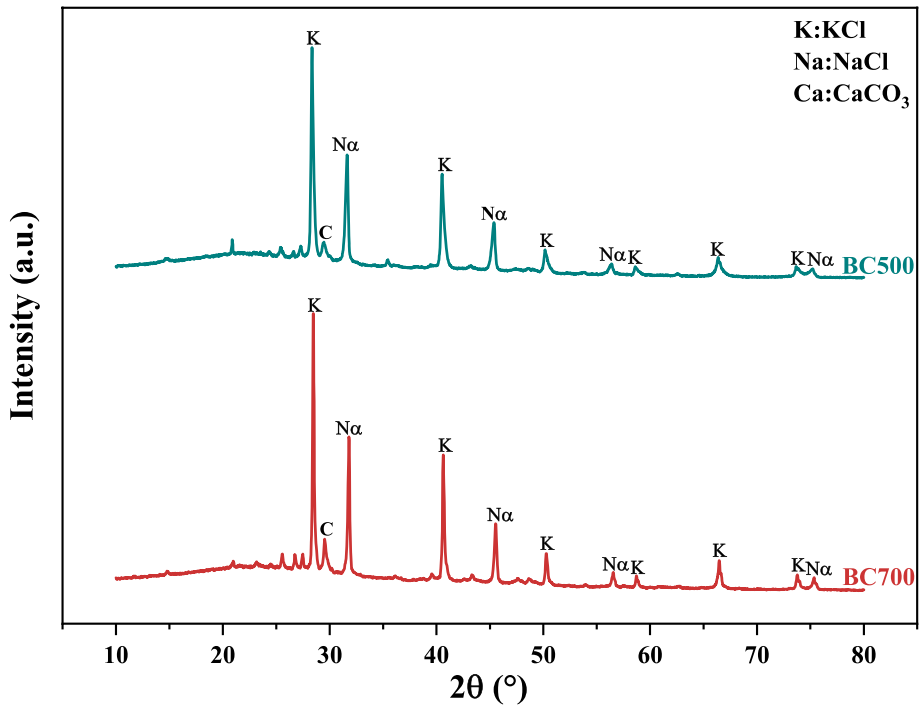

Fig. 2 X-ray diffraction spectra of BC500 and BC700

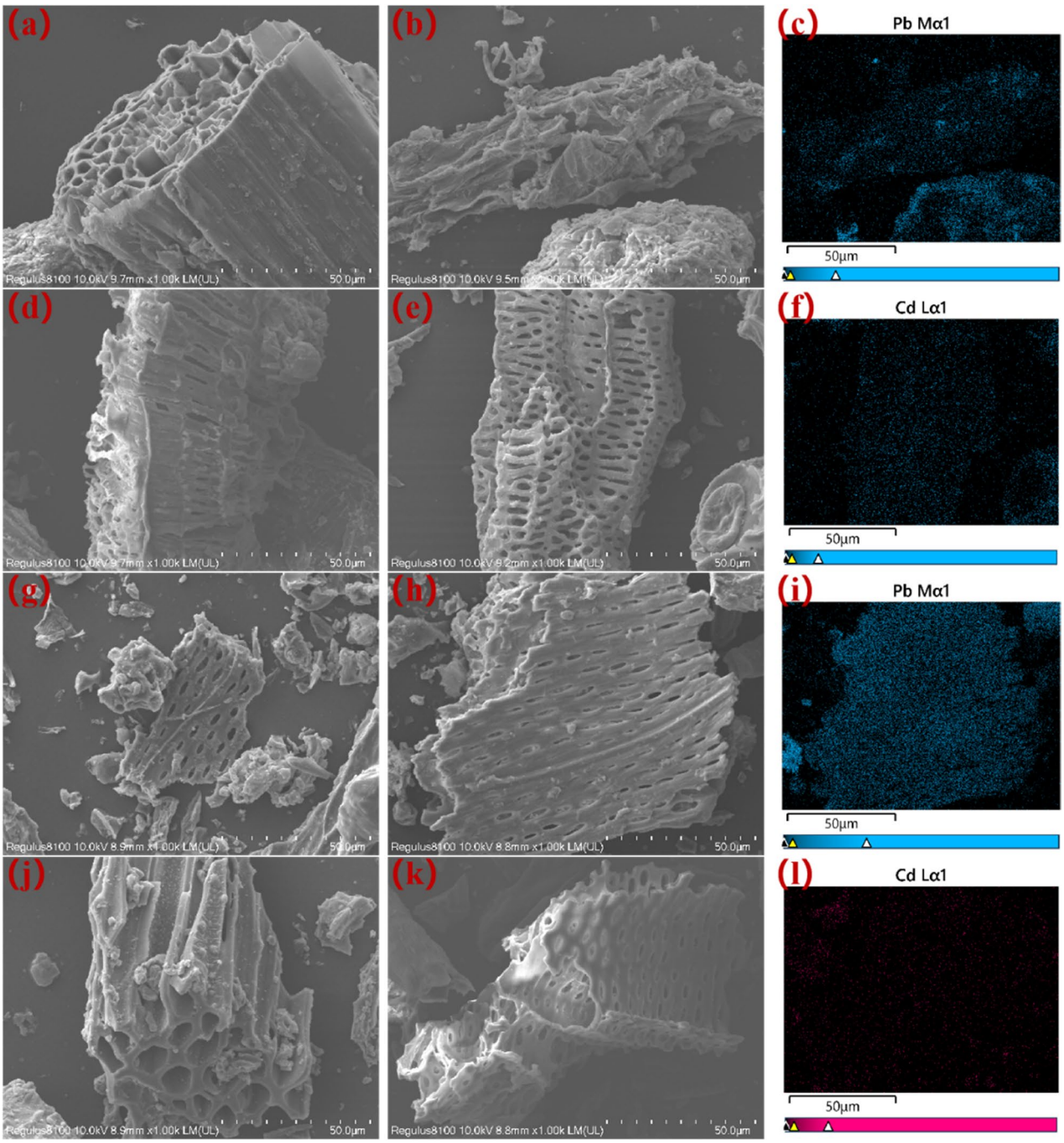

Fig. 3 SEM–EDS element mapping of obtained biochar samples. **a** and **d** fresh samples of BC500 before adsorption; **b** and **e** BC500 after adsorption of Pb^{2+} and Cd^{2+}; **c** and **f** distribution of Pb and Cd on BC500 after adsorption; **g** and **j** fresh samples of BC700; **h** and **k** BC700 after adsorption of Pb^{2+} and Cd^{2+}; **i** and **l** distribution of Pb and Cd on BC700 after adsorption

3.2 Pb and Cd adsorption characteristics

3.2.1 Effect of initial pH of solution on adsorption capacity

The initial pH significantly influences the adsorption capacity and equilibrium pH of biochars (Fig. 4). As the solution's initial pH rose from 1.5 to 6.5, the adsorption capacity for Pb^{2+} and Cd^{2+} initially increased rapidly and then leveled off. Both the adsorption capacity and equilibrium pH stabilized at pH 5.5, which is consistent with prior studies (Lian et al. 2020). At lower pH values, protonation increased the positive charge density

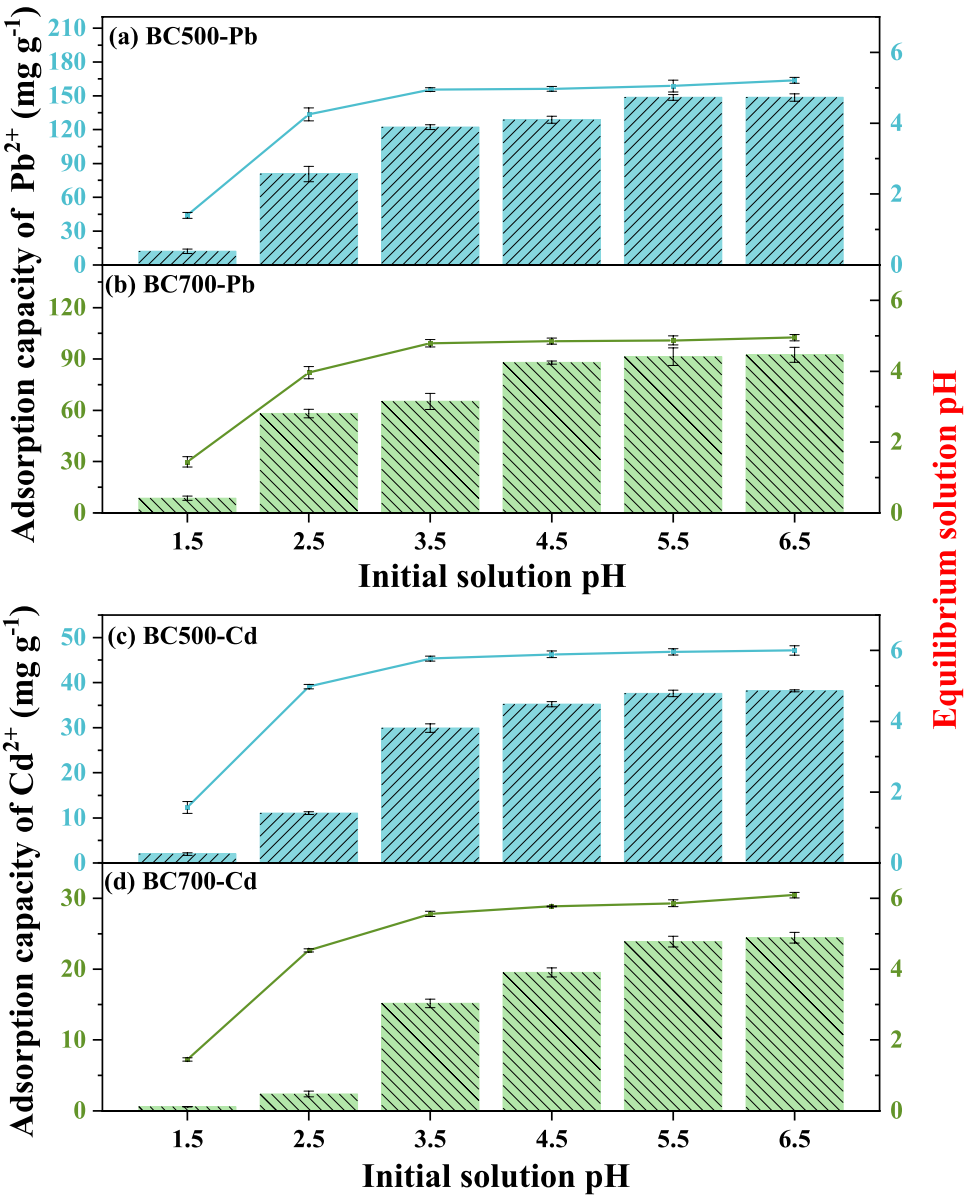

Fig. 4 Effect of initial solution pH on adsorption capacity and equilibrium solution pH of biochars. **a**, **b** Pb^{2+} onto BC500 and BC700; **c**, **d** Cd^{2+} onto BC500 and BC700

on the biochar surface, causing electrostatic repulsion of Pb^{2+} and Cd^{2+}. Simultaneously, H^+ competed with Pb^{2+} and Cd^{2+} for adsorption sites, resulting in a lower removal rate. With increasing pH, the biochar's adsorption capacity improved. This could be attributed to surface deprotonation and dissociation of functional groups at high pH, which renders the biochar surface more negatively charged and facilitates the formation of surface complexes with Pb^{2+} and Cd^{2+}. Additionally, the rise in basic groups on the biochar surface promoted the stable mineral precipitation of Pb^{2+} and Cd^{2+} (Khan et al. 2020; Yuan et al. 2020).

3.2.2 Adsorption kinetics

Figure 5 shows the time-dependent adsorption curve for Pb^{2+} and Cd^{2+} on biochar over 24 h. During the initial 0–60 min, the high chemical concentrations of Cd^{2+} and Pb^{2+}, combined with abundant adsorption sites on the biochar surface, accelerated the adsorption process. As the concentrations of Cd^{2+} and Pb^{2+} in the solution

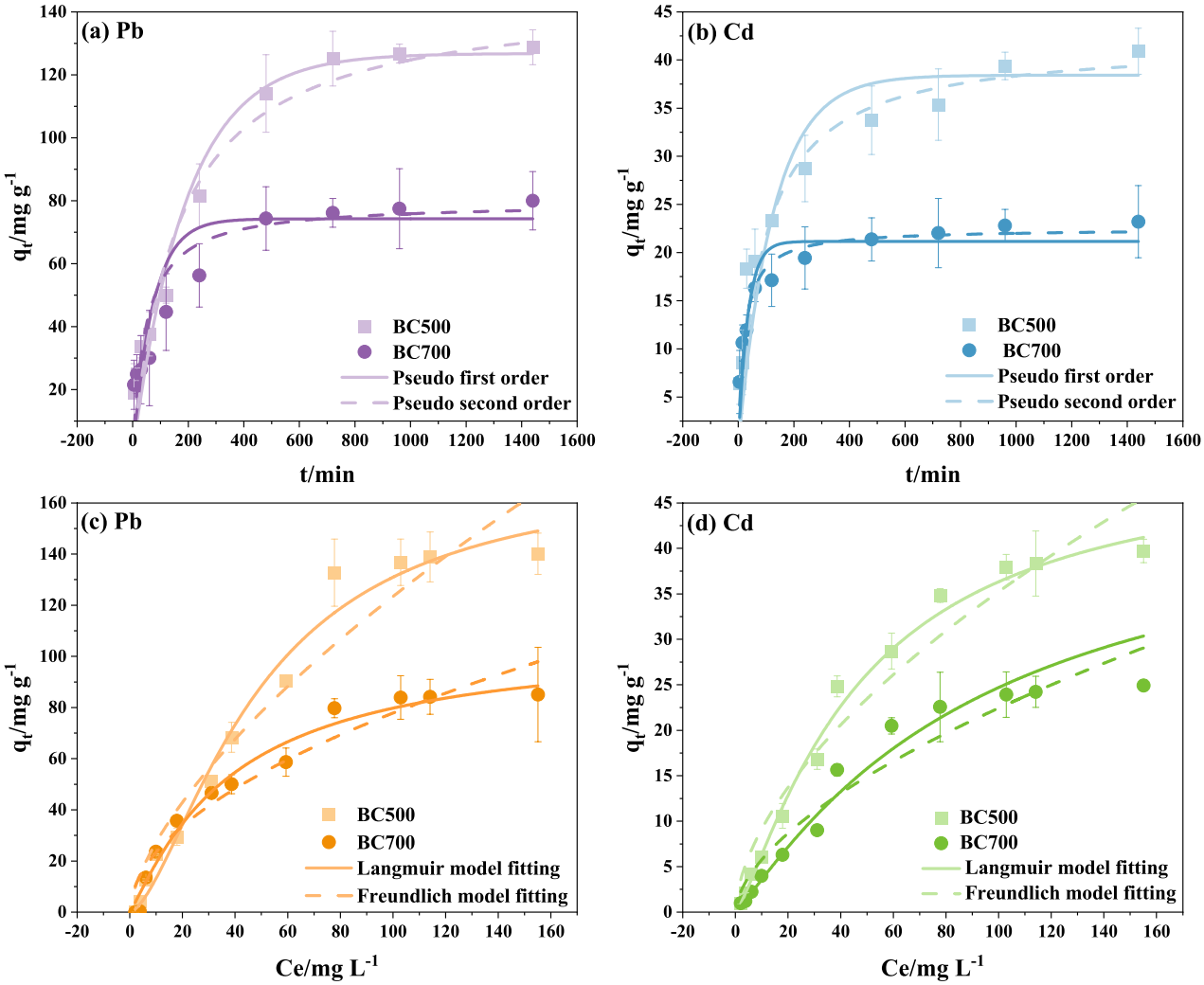

Fig. 5 Adsorption kinetics and isotherms for Pb and Cd onto BC500 and BC700. **a**, **b** adsorption kinetics and **c**, **d** adsorption isotherm

underwent reduction and depletion, the chemical potential gradually decreased, and the most active adsorption sites became occupied. Consequently, the rate of desorption increased, although it consistently stayed below the adsorption rate. Between 3 and 24 h, the adsorption effect significantly declined, indicating an approach to stagnation in the adsorption rate growth and the achievement of dynamic equilibrium with desorption (Wang et al. 2023). The model parameters indicated a better fit for the pseudo-second-order model ($0.888 \leq R^2 \leq 0.957$) compared to the pseudo-first-order model ($0.828 \leq R^2 \leq 0.948$) (Table S2). This suggested that chemical adsorption predominantly occurs on the biochars due to the presence of uniformly distributed pores and various oxygen-containing functional groups (Wang et al. 2023; Yan et al. 2020). BC500 exhibited maximum adsorption capacities (q_e) of 127.337 mg g^{-1} for Pb^{2+} and 35.844 mg g^{-1} for Cd^{2+}, while BC700 showed capacities of 75.564 mg g^{-1} for Pb^{2+} and 20.931 mg g^{-1} for Cd^{2+}. Notably, the derivative coefficient (h) of BC700 was higher than that for BC500, indicating a more rapid reaction rate for BC700 in the initial stage of adsorption.

3.2.3 Adsorption isotherm

The adsorption isotherm parameters and curves for Pb^{2+} and Cd^{2+} on BC500 and BC700 are shown in Fig. 5. Table 2 indicates that both the Langmuir and Freundlich isothermal adsorption models effectively simulated the adsorption process of biochar. The Langmuir model ($0.977 \leq R^2 \leq 0.992$) demonstrated a better fit with the adsorption process of BC500 and BC700 biochar than the Freundlich model ($0.923 \leq R^2 \leq 0.946$). The Langmuir model, suitable for single-layer homogeneous adsorption, suggested that the adsorption of BC500 and BC700 corresponded to a monolayer adsorption process (Deng et al. 2020). The parameter 1/n reflects the

Table 2 Isothermal adsorption parameters of Pb^{2+} and Cd^{2+} by BC500 and BC700

Heavy mental	Biochar	Langmuir			Freundlich		
		Q_{max}	K_1	R^2	K_f	$1/n$	R^2
		(mg g^{-1})	(L mg^{-1})		(mg g^{-1})		
Pb^{2+}	BC500	159.522	0.00041	0.984	4.603	0.497	0.923
	BC700	98.400	0.00462	0.977	5.756	0.394	0.928
Cd^{2+}	BC500	46.736	0.00506	0.992	2.364	0.587	0.946
	BC700	28.026	0.00224	0.982	1.482	0.590	0.924

adsorption affinity of biochar for heavy metal ions. When $0.1 < 1/n < 0.5$, it indicates that heavy metal ions are easily adsorbed by adsorbents. Table 2 reveals that both BC500 and BC700 exhibited a higher adsorption affinity for Pb^{2+} compared to Cd^{2+}. According to the maximum adsorption capacity calculated by the Langmuir model, BC500 had a maximum adsorption capacity of 159.5 mg g^{-1} for Pb^{2+} and 46.7 mg g^{-1} for Cd^{2+}, while BC700 had a maximum adsorption capacity of 98.4 mg g^{-1} for Pb^{2+} and 28.0 mg g^{-1} for Cd^{2+}. Under comparable experimental conditions, the maximum adsorption capacities of BC500 for Pb^{2+} and Cd^{2+} in this study surpassed those of biochars (0.3–36 mg g^{-1} for Cd, 2.4–147 mg g^{-1} for Pb) derived from crop straw, grass, wood, manure, sewage sludge, and even chemically modified biochars, as reported in a review study by Inyang et al. (2016). Therefore, the higher adsorption capacity, coupled with more stable fraction of adsorbed Cd and Pb on biochar surface, indicated that BC500 could serve as an effective adsorbent for the removal of Pb and Cd from wastewater.

3.2.4 Adsorption morphology

The speciation distribution of adsorbed Pb^{2+} and Cd^{2+} by biochar is presented in Fig. 6 and Table S3. The majority of Pb^{2+} and Cd^{2+} adsorbed by both BC500 and BC700 were in the acid-soluble state. Specifically, BC700 exhibited over 80% of Pb^{2+} and Cd^{2+} in the acid-soluble state, with stable adsorption percentages lower than those of BC500. In BC500, stable Pb^{2+} and Cd^{2+} accounted for 25.2% and 20.5%, respectively, while in BC700, these percentages decreased to 16.1% for Pb^{2+} and 1.0% for Cd^{2+}. The higher exchangeable Cd on BC500 was due to its higher content of dissolvable cations that could be exchanged with Cd in aqueous solutions (Lian et al. 2020; Wu et al. 2019). In contrary, the content of generally stable Cd and Pb on BC500 were significantly higher than that on BC700. This observation implies the formation of mineral crystals and decomposition of carboxylic groups on BC500. When considering the application of biochar for remediating soils contaminated with heavy metals, it is essential to prioritize the stability of heavy metal adsorption by biochar. This emphasis is crucial to prevent both the desorption of the metals and their subsequent uptake by plants. This suggests that BC500 may be more suitable for the immobilization of Pb^{2+} and Cd^{2+} in contaminated soil.

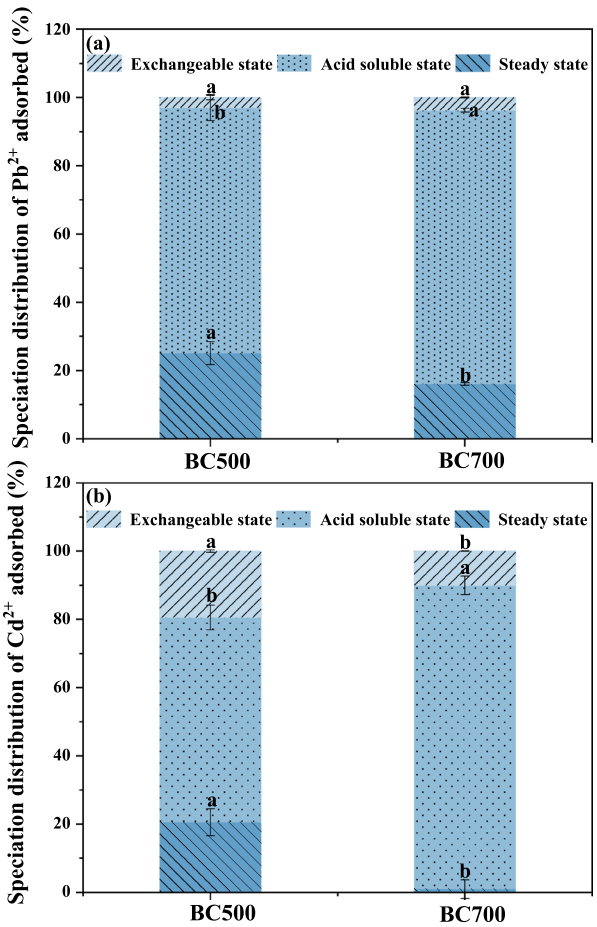

Fig. 6 Percentage distribution of adsorbed Pb^{2+} **a** and Cd^{2+} **b** on BC500 and BC700. The bars represent standard deviation and different letters above the blocks indicate a significant difference among the treatments at $P < 0.05$

Table 3 Changes in the yield and quality of Chinese cabbages leaves following biochar soil amendment

Trea ment	Biomass (g pot^{-1})	Soluble sugar (g kg^{-1})	PAHs [a] (ng g^{-1})	*N* [b] (g kg^{-1})	*P*(g kg^{-1})	K (g kg^{-1})	Total *N* uptake [c] (mg pot^{-1})	Total *P* uptake mg pot^{-1})	Total K uptake (mg·pot^{-1})
CK	16.0 ± 4.4b	1.65 ± 0.44c	9.19 ± 1.06c	13.66 ± 0.02c	9.09 ± 0.82a	26.08 ± 0.36b	38.25 ± 10.01c	21.29 ± 4.94b	61.59 ± 15.75c
BC500	35.1 ± 14.9a	3.56 ± 0.04a	20.79 ± 3.62b	17.49 ± 0.16a	8.97 ± 0.62a	30.24 ± 0.31a	109.45 ± 11.7a	47.60 ± 7.68a	159.48 ± 13.99a
BC700	29.7 ± 0.3a	3.72 ± 0.06a	30.35 ± 2.51a	15.13 ± 0.53b	9.7 ± 0.70a	27.00 ± 1.95ab	80.08 ± 3.49b	43.36 ± 3.40a	120.56 ± 7.87b

Values are presented as mean ± standard deviation ($n = 4$). Different lowercase letters within a single column indicate a significant difference between the treatments at $p < 0.05$. BC500 and BC700, soil amendments with 1 % biochar produced at 500 °C and 700 °C, respectively

[a] The concentrations of 16 PAH monomers (mg kg^{-1}) are provided in Table S4

[b] The concentrations of nutrients in Chinese cabbage leaves

[c] Total uptake of nutrients in Chinese cabbage leaves (biomass × concentration)

3.2.5 Adsorption mechanisms

After the adsorption of Pb^{2+} and Cd^{2+}, the aromaticity C=C stretching vibration peak of BC 500 shifted from 1622.51 cm^{-1} to 1588.88 cm^{-1} and 1609.93 cm^{-1}, respectively (Fig. S4). Similarly, the C=C stretching vibration peaks of BC700 shifted from 1632.54 cm^{-1} to 1616.82 cm^{-1}, suggesting C=C group involvement in the adsorption process with π bond coordination with heavy metal ions (Park et al. 2019). The –COO– at 1431 ~ 1438 cm^{-1} also transferred, possibly due to ion exchange between cations in carboxyl salts and Pb^{2+} and Cd^{2+}. The C–O–C, initially at 1111.67 ~ 1114.6 cm^{-1}, shifted to 1047.7 cm^{-1}, 1048.74 cm^{-1}, 1047.31 cm^{-1}, and 1044.5 cm^{-1}, indicating the participation of the C–O–C group in the adsorption of Pb^{2+} and Cd^{2+} (Cui et al. 2016). Therefore, it could be concluded that aromatic C=C and oxygen-containing functional groups on biochar's surface adsorbed Pb^{2+} and Cd^{2+} through M^{2+}-π interaction, ion exchange, and complexation.

The XRD patterns revealed carbonate precipitation of Pb^{2+} on biochar after adsorption, sulfide precipitation on BC500, and water-insoluble lead oxide on BC700 (Fig. S5). This indicated biochar fixed Pb^{2+} through precipitation, clarifying the generally higher stablility of Pb fractions on BC500 with no significant changes in exchangeable Pb between BC500 and BC700.

SEM–EDS was utilized to investigate the surface micro-morphology and element composition of post-sorption biochar, providing additional insights into the Pb^{2+} and Cd^{2+} adsorption mechanism. The SEM images and elemental mapping in Fig. 3 revealed that precipitates and compounds of Pb^{2+} and Cd^{2+} covered the surface and pores of biochar. The SEM–EDS spectrum in Fig. S6 further confirmed the biochar's adsorption capacity for Pb^{2+} and Cd^{2+}. In summary, the stable fractions of Cd and Pb immobilized by BC500 were 2.6 and 35.0 times higher, respectively, than those immobilized by BC700, as indicated by the sequential leaching results (Fig. 6 and Table S3). This suggested that the majority of Pb and Cd associated with BC500 pose a lower risk in the context of the soil environment (Shen et al. 2019).

3.3 Plant yield, quality, and toxic elements

3.3.1 Changes in plant growth and soil properties

The results indicated a significant enhancement in leaf biomass and quality of Chinese cabbage with the addition of biochar to the soil. In comparison to the control (CK), the yields of BC500 and BC700 processing increased by 119% and 87%, respectively, and the soluble sugar content enhanced by 116% and 125% (Table 3, Fig. S7). These improvements can be attributed to the addition of biochar, which increased soil pH and nutrient availability, while also significantly reducing the bioavailability of the Pb and Cd. In detail, comparing to CK, the soil pH increased by 0.96–1.03 unit, and the availability of soil K was elevated by 2.8–3.2 times under the biochar treatment. Additionally, a significant increase in soil available P was observed, rising by 21% only under BC500 compared to CK (Table 4). Hence, a significant elevation in N and K content was observed, coupled with a two to threefold increase in the total uptake of N, P, and K within cabbage leaves (Table 3). This phenomenon markedly contributed to substantial improvements in both yield and quality. The current investigation revealed a more advantageous response in terms of plant yield and nutrient content under BC500 compared to BC700. The improved performance can be attributed to the direct nutrient supplementation provided by biochar. Additionally, it may be influenced by the increased availability of micronutrients and soluble organic carbon from biochar, which, although not measured in this study, have been shown in previous research to stimulate soil microorganisms and enhance nutrient cycling in the soil (Azeem et al. 2023). Consequently, under BC500, there was a notable increase in soil SMBC by 66% and SMBN by 110%, while under BC700, the increase was 43% for SMBC and 81% for SMBN, as compared to the CK (Table 4). In general, soil microbial biomass (SMB) plays a crucial role in sustaining soil functions by reflecting the dynamics of microbial metabolic activity and regulating the availability of soil nutrients (Zhang et al. 2016). The observed increase in SMB suggested that the biochar produced in this study, despite its relatively high content of PAHs, did not exhibit toxic effects on soil microorganisms. Instead, it appeared to have stimulated the growth of soil microbial biomass and enhanced the content of soil bio-available nutrients.

3.3.2 Changes in Pb and Cd in soil and cabbage

In accordance with the findings from adsorption experiments, the application of biochar resulted in a significant reduction in the bioavailability of Pb and Cd in the contaminated soil. Furthermore, the passivation effect of biochar on Pb was observed to be greater than its effect on Cd. Comparative analysis with the CK revealed that the $CaCl_2$ extractable pool of Pb and Cd in soil was substantially immobilized by 95–96% and 69–73% (Fig. 7), respectively, following biochar soil amendment. Consequently, the Pb and Cd concentrations in cabbage leaves were decreased by 83–85% and 29–39% (Fig. 7), respectively. Notably, the Pb and Cd immobilization capacity of biochar remained consistent across different pyrolysis temperatures. This finding could be attributed to the uniform impact of biochar treatments in increasing soil pH. Soil pH has been recognized as a dominant factor regulating the mobility of heavy metals in soil (Kicińska et al.

Table 4 Changes in soil properties following biochar addition after harvest of Chinese cabbage

Treatment	pH	SOM (g kg^{-1})	TN (g kg^{-1})	Available K (mg kg^{-1})	Available P (mg kg^{-1})	SMBC (mg kg^{-1})	SMBN (mg kg^{-1})
CK	4.52 ± 0.03b	29.33 ± 1.83b	1.65 ± 0.02b	245.3 ± 26.3c	40.43 ± 1.88b	493.1 ± 44.5c	45.0 ± 10.7b
BC500	5.48 ± 0.07a	31.69 ± 0.30a	1.89 ± 0.01a	784.7 ± 12.6a	49.11 ± 2.01a	820.4 ± 39.4a	94.6 ± 2.2a
BC700	5.55 ± 0.09a	32.53 ± 0.19a	1.93 ± 0.10a	701.0 ± 38.0b	36.05 ± 3.14b	704.2 ± 7.5b	81.3 ± 3.6a

Values are presented as mean ± standard deviation (n = 4). Different lowercase letters within a single column indicate a significant difference between the treatments at $p < 0.05$

SOM, soil organic matter; TN, total nitrogen; SMBC, soil microbial biomass carbon; SMBN, soil microbial biomass nitrogen; BC500 and BC700, soil amendments with 1% biochar produced at 500 °C and 700 °C, respectively

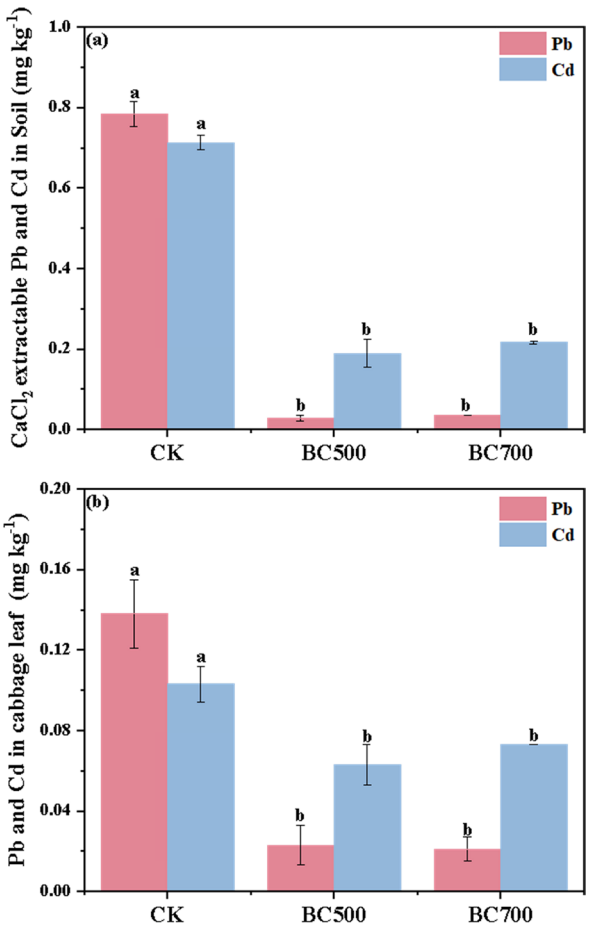

Fig. 7 Changes in soil $CaCl_2$-extractable Pb and Cd (**a**) and concentrations of Pb and Cd in cabbage leaves (**b**) following biochar addition. The bars represent standard deviation and different letters above the blocks indicate a significant difference among the treatments at $P < 0.05$

2022). The liming effects in soil were known to enhance the adsorption of Cd and Pb onto the surfaces of soil particles (He et al. 2021a). Precipitation of most toxic metals occurs with low mobility when soil pH exceeds 6.5 (Kicińska et al. 2022). Consequently, the increase in soil pH due to the alkaline nature of biochar led to a reduction in soil Cd and Pb mobility, resulting in decreased availability for plant uptake (Albert et al. 2021). In this study, the biochar introduced oxygen-containing functional groups, including carboxyl and hydroxyl groups (Fig. 1). These groups confer negative charges, such as $-COO^-$ and $-O^-$, to the soil, thereby facilitating the stable immobilization of heavy metals through surface binding and adsorption processes for an extended period (Liao et al. 2023).

Beyond the positive effects, this study highlights that the environmental risks associated with the use of biochar derived from honeydew melon vines. Notably, it significantly promoted PAHs accumulation in cabbage leaves, with concentrations increasing from 9.19 ng g^{-1} in CK to 20.79 ng g^{-1} under BC500 and 30.35 ng g^{-1} under BC700, respectively. This finding is consistent with Wang et al. (2018b), who observed that both commercial and laboratory-produced biochars significantly increased PAHs levels in Chinese cabbage leaves in field trials, with concentrations from 98 to 1494 μg kg^{-1}, potentially posing health risks. Khan et al. (2015a; 2015b) noted that PAHs concentrations in lettuce grown with pulp sludge biochar, produced at 450 °C, 500 °C, and 550 °C, varied from 10.3 to 87.9 ng g^{-1} in a controlled growth chamber. In this study, the primary increase in PAHs was attributed to a rise in less toxic compounds, notably acenaphthene and naphthalene. These compounds accounted for 94% and 93% of the total PAHs content under the BC500 and BC700 treatments, respectively, with acenaphthene contributing 6% and naphthalene 7%. (Table S4). Wang et al. (2018b) analyzed 80 vegetable samples from markets in Beijing, China and found an average total PAHs concentration of 30.1 ng g^{-1} in Chinese cabbage, suggesting that the levels of PAHs in this study might be within acceptable limits. Benzo**a**pyrene (BaP) in cabbage leaves was undetectable, well below the regulatory limit of 5 ng g^{-1} established by the China Food and Drug Administration (CFDA 2017). This finding suggested the necessity for further research to assess the long-term impacts of PAHs from biochar application on plant accumulation. Consequently, the higher yield of cabbage and the increased soil microbial biomass, along with the lower

PAHs content in the leaves, indicated that pyrolysis at 500 °C is more suitable and safer for producing biochar from honeydew melon vines containing plastic hanging rope than pyrolysis at 700 °C. This finding is consistent with previous studies by López et al. (2011) and Yuan et al. (2011), who also suggested that 500 °C as the ideal temperature for pyrolyzing plastic and biomass wastes, optimizing conversion efficiency and the product quality.

4 Conclusion

This study revealed that co-pyrolysis technology effectively converted honeydew melon vines and plastic hanging ropes into biochar materials for Pb and Cd stabilization in liquid solution and contaminated soil. The biochar's adsorption capacity for Pb and Cd in solution was temperature-dependent, with BC500 outperforming conventional biochars, suggesting its potential for environmental remediation. Pot experiment results indicated biochar soil amendment significantly promoted Chinese cabbage yield and immobilized Pb and Cd in contaminated soil. However, the PAHs content in BC700 approached critical value of IBI leading to an enrichment of PAHs in Chinese cabbage. Nonetheless, Benzo**a**pyrene (BaP), a potent carcinogen, was not detected in cabbage leaves. A comprehensive analysis suggested that a pyrolysis temperature of 500 °C was more suitable for treating plastic-contaminated crop straw, as it strikes a balance between biochar yield, nutrient content, heavy metal immobilization, promotion of plant growth, and environmental safety, surpassing the performance at both 300 °C and 700 °C. Future research should focus on advancing large-scale pyrolysis technologies, enforcing the control of PAHs during pyrolysis, and evaluating the long-term impacts and potential environmental risks of biochar application for soil amendment.

Abbreviations

PAHs	Polycyclic Aromatic Hydrocarbons
BC	Biochar
BC500	Biochar produced at 500 ℃
BC700	Biochar produced at 700 ℃
BET	Brunauer-Emmett-Teller
EBC	European Biochar Certificate
FTIR	FT-IR Fourier-transform infrared spectroscopy
HMs	Heavy metals
IBI	International Biochar Initiative
ICP-OES	Inductively coupled plasma-optical emission spectrometry
ICP-MS	Inductively coupled plasma-mass spectromety
SEM-EDS	Scanning electron microscope-energy-disper sive spectroscopy
SMBC	Soil microbial biomass carbon
SMBN	Soil microbial biomass nitrogen
SOM	Soil organic matter
XRD	X-ray difractometry

Supplementary Information

The online version contains supplementary material available at https://doi.org/10.1007/s42773-024-00382-7.

Supplementary Material 1. Additional figures and tables.

Acknowledgements

The authors express their appreciation to the editor as well as the anonymous reviewers for their remarks and constructive recommendations towards enhancing the quality of this manuscript.

Author contributions

QY: Investigation, analysis, data collection, and writing the draft manuscript. XZ: Investigation, methodology, review and editing. TG, XG, JW, and ST: Investigation, analysis. BM: Methodology and data collection. LX, SJ, JZ: Review and editing. RB, LL: Project administration and supervision, funding acquisition, writing the draft manuscript, review and editing. All authors contributed to the article and approved the submitted version.

Funding

This work was supported by the Science and Technology Innovation Program of Jiangsu province, China for "Carbon Dioxide Emission Peaking and Carbon Neutrality" (BE2022423 and BE2022307); and CHN-2152, 22/0013 SINOGRAIN III; Natural Science Foundation of Jiangsu Province (BK20231477) and Guangdong Provincial Housing and Urban–Rural Development (2023-K33-415203).

Availability of data and materials

The datasets used or analyzed during the current study are available from the corresponding author on reasonable request.

Declarations

Competing interests

The authors have no competing interests to declare that are relevant to the content of this article.

Author details

[1]Institute of Resources, Ecosystem and Environment of Agriculture, Nanjing Agricultural University, 1 Weigang, Nanjing 210095, China. [2]Jiangsu Collaborative Innovation Center for Solid Organic Waste Resource Utilization, Nanjing Agricultural University, 1 Weigang, Nanjing 210095, China. [3]Institute of Food Safety and Nutrition, Jiangsu Academy of Agricultural Sciences, Nanjing 210014, China. [4]Biomass Group, College of Engineering, Nanjing Agricultural University, No. 40 Dianjiangtai Road, Nanjing 210031, China. [5]School of Materials Science and Engineering, University of New South Wales, Kensington, NSW 2052, Australia.

Received: 4 March 2024 Revised: 18 July 2024 Accepted: 24 August 2024
Published online: 21 November 2024

References

Albert HA, Li X, Jeyakumar P, Wei L, Huang L, Huang Q, Kamran M, Shaheen SM, Hou D, Rinklebe J, Liu Z, Wang H (2021) Influence of biochar and soil properties on soil and plant tissue concentrations of Cd and Pb: a meta-analysis. Sci Total Environ 755:142582. https://doi.org/10.1016/j.scitotenv.2020.142582

Azeem M, Sun TR, Jeyasundar PGSA, Han RX, Li H, Abdelrahman H, Shaheen SM, Zhu YG, Li G (2023) Biochar-derived dissolved organic matter (BDOM) and its influence on soil microbial community composition, function, and activity: a review. Crit Rev Env Sci Technol 53:1912–1934. https://doi.org/10.1080/10643389.2023.2190333

Aziz S, Bibi S, Hasan MM, Biswas P, Ali MI, Bilal M, Chopra H, Mukerjee N, Maitra S (2023) A review on influence of biochar amendment on soil processes and environmental remediation. Biotechnol Genet Eng 1:1–35. https://doi.org/10.1080/02648725.2022.2122288

Bao S (2000) Soil agrochemical analysis, 3rd edn. Agriculture Press, BeiJing

Buema G, Lupu N, Chiriac H, Ciobanu G, Bucur RD, Bucur D, Favier L, Harja M (2021) Performance assessment of five adsorbents based on fly ash for removal of cadmium ions. J Mol Liq 333:115932. https://doi.org/10.1016/j.molliq.2021.115932

Buss W, Hilber I, Graham MC, Mašek O (2022) Composition of PAHs in biochar and implications for biochar production. ACS Sustain Chem Eng 10:6755–6765. https://doi.org/10.1021/acssuschemeng.2c00952

CFDA (China Food and Drug Administration) (2017) National Food Safety Standard Limits of Contaminants in Food (GB 2762–2017) . http://www.mengyin.gov.cn/info/4600/89286.htm. Accessed 2 Jan 2024

Cui X, Fang S, Yao Y, Li T, Ni Q, Yang X, He Z (2016) Potential mechanisms of cadmium removal from aqueous solution by Canna indica derived biochar. Sci Total Environ 562:517–525. https://doi.org/10.1016/j.scitotenv.2016.03.248

Dai L, Lata S, Cobb K, Zou R, Lei H, Chen P, Ruan R (2024) Recent advances in polyolefinic plastic pyrolysis to produce fuels and chemicals. J Anal Appl Pyrolysis 180:106551. https://doi.org/10.1016/j.jaap.2024.106551

Deng Y, Huang S, Dong C, Meng Z, Wang X (2020) Competitive adsorption behaviour and mechanisms of cadmium, nickel and ammonium from aqueous solution by fresh and ageing rice straw biochars. Bioresour Technol 303:122853. https://doi.org/10.1016/j.biortech.2020.122853

EBC (European Biochar Certificate) (2023) European Biochar Certificate Guidelines for a sustainable production of biochar. https://www.european-biochar.org/en/. Accessed 2 Jan 2024

FAO Statistical Yearbook (2022) Food and Agriculture Organization of the United Nations. https://www.fao.org/home/zh. Accessed 2 Jan 2024

Hale SE, Lehmann J, Rutherford D, Zimmerman AR, Bachmann RT, Shitumbanuma V, O'Toole A, Sundqvist KL, Arp HPH, Cornelissen G (2012) Quantifying the total and bioavailable polycyclic aromatic hydrocarbons and dioxins in biochars. Environ Sci Technol 46:2830–2838. https://doi.org/10.1021/es203984k

Hassan H, Hameed BH, Lim JK (2020) Co-pyrolysis of sugarcane bagasse and waste high-density polyethylene: Synergistic effect and product distributions. Energy 191:116545. https://doi.org/10.1016/j.energy.2019.116545

He LL, Huang DY, Zhang Q, Zhu HH, Xu C, Li B, Zhu QH (2021a) Meta-analysis of the effects of liming on soil pH and cadmium accumulation in crops. Ecotoxicol Environ Saf 223:112621. https://doi.org/10.1016/j.ecoenv.2021.112621

He T, Zhong S, Liu C, Shujaa A, Zhang B (2021b) Enhancing hydrocarbon production via ex-situ catalytic co-pyrolysis of biomass and high-density polyethylene: Study of synergistic effect and aromatics selectivity. Waste Manage 128:189–199. https://doi.org/10.1016/j.wasman.2021.04.058

Huang D (2020) Measures for the management of agricultural films. https://www.gov.cn/zhengce/zhengceku/2020-08/02/content_5531956.htm. Accessed 2 Jan 2024

Huang T, Hu L, Wu J, Zhang W, Mao L (2023) Characteristics of biochar and adsorption of Cd^{2+} in bovine bones at different pyrolysis temperatures. J Agro-Environ Sci 42(7):1632–1644. https://doi.org/10.11654/jaes.2023-0045

IBI (International Biochar Initiative) (2015) CERTIFICATION PROGRAM. https://biocharinternational.org/standard-certification-training/certification-program/. Accessed 2 Jan 2024

Inyang MI, Gao B, Yao Y, Xue Y, Zimmerman A, Mosa A, Pullammanappallil P, Ok YS, Cao X (2016) A review of biochar as a low-cost adsorbent for aqueous heavy metal removal. Crit Rev Env Sci Technol 46:406–433. https://doi.org/10.1080/10643389.2015.1096880

Kai X, Yang T, Shen S, Li R (2019) TG-FTIR-MS study of synergistic effects during co-pyrolysis of corn stalk and high-density polyethylene (HDPE). Energy Convers Manage 181:202–213. https://doi.org/10.1016/j.enconman.2018.11.065

Khan A, Mirza M, Fahlman B, Rybchuk R, Yang J, Harfield D, Anyia AO (2015a) Mapping thermomechanical pulp sludge (TMPS) biochar characteristics for greenhouse produce safety. J Agric Food Chem 63(5):1648–1657. https://doi.org/10.1021/jf502556t

Khan R, Chu J, Margrave J, Hauge R, Smalley R (2005) Free radical chemistry during slow pyrolysis of solid fuels. Energy Source 27(3):279–298. https://doi.org/10.1080/009083190519005

Khan S, Waqas M, Ding F, Shamshad I, Arp HPH, Li G (2015b) The influence of various biochars on the bioaccessibility and bioaccumulation of PAHs and potentially toxic elements to turnips (Brassica rapa L.). J Hazard Mater 300:243–253. https://doi.org/10.1016/j.jhazmat.2015.06.050

Khan ZH, Gao M, Qiu W, Song Z (2020) Properties and adsorption mechanism of magnetic biochar modified with molybdenum disulfide for cadmium in aqueous solution. Chemosphere 255:126995. https://doi.org/10.1016/j.chemosphere.2020.126995

Kicińska A, Pomykała R, Izquierdo-Diaz M (2022) Changes in soil pH and mobility of heavy metals in contaminated soils. Eur J Soil Sci 73(1):e13203. https://doi.org/10.1111/ejss.13203

Kou W, Wang W, Jiang C, Zhou L, Wu K (2020) Integrated cultivation technology of water and fertilizer for chestnut pumpkin greenhouse in northern Anhui. Chin Melon Veg 33(11):102–104. https://doi.org/10.16861/j.cnki.zggc.2020.0296

Lanorte A, De Santis F, Nolè G, Blanco I, Loisi RV, Schettini E, Vox G (2017) Agricultural plastic waste spatial estimation by Landsat 8 satellite images. Comput Electron Agric 141:35–45. https://doi.org/10.1016/j.compag.2017.07.003

Li X, Pan C, Song Y, Yuan X, Cheng H, Ni N, Wang Z (2023) Co-pyrolysis technology and high-value utilization of typical plastic and biomass waste. Environ Res 36:1765–1678. https://doi.org/10.13198/j.issn.1001-6929.2023.08.01

Lian W, Yang L, Joseph S, Shi W, Bian R, Zheng J, Li L, Shan S, Pan G (2020) Utilization of biochar produced from invasive plant species to efficiently adsorb Cd (II) and Pb (II). Bioresour Technol 317:124011. https://doi.org/10.1016/j.biortech.2020.124011

Liao W, Zhang X, Ke S, Shao J, Yang H, Zhang S, Chen H (2022) Effect of different biomass species and pyrolysis temperatures on heavy metal adsorption, stability and economy of biochar. Ind Crops Products 186:115238. https://doi.org/10.1016/j.indcrop.2022.115238

Liao W, Zhang X, Ke S, Shao J, Yang H, Zhang S, Chen H (2023) The influence of biomass species and pyrolysis temperature on carbon-retention ability and heavy metal adsorption property during biochar aging. Fuel Process Technol 240:107580. https://doi.org/10.1016/j.fuproc.2022.107580

Lin X, Chen X, Fu P, Tang B, Bi D (2023) Highly efficient production of monocyclic aromatics from catalytic co-pyrolysis of biomass and plastic with nitrogen-doped activated carbon catalyst. Chem Eng J 474:145783. https://doi.org/10.1016/j.cej.2023.145783

Liu X, Burra KG, Wang Z, Li J, Che D, Gupta AK (2020) On deconvolution for understanding synergistic effects in co-pyrolysis of pinewood and polypropylene. Appl Energy 279:115811. https://doi.org/10.1016/j.apenergy.2020.115811

López A, de Marco I, Caballero BM, Laresgoiti MF, Adrados A (2011) Influence of time and temperature on pyrolysis of plastic wastes in a semi-batch reactor. Chem Eng J 173:62–71. https://doi.org/10.1016/j.cej.2011.07.037

Lu Z, Gao P (2019) Analysis of climate suitability of Wallace melon in Dengkou County. Chin Melon Veg 32:129–133. https://doi.org/10.16861/j.cnki.zggc.2019.0157

Ma Z, Yang Y, Ma Q, Zhou H, Luo X, Liu X, Wang S (2017) Evolution of the chemical composition, functional group, pore structure and crystallographic structure of bio-char from palm kernel shell pyrolysis under different temperatures. J Anal Appl Pyrolysis 127:350–359. https://doi.org/10.1016/j.jaap.2017.07.015

Ma Z, Zhang Y, Shen Y, Wang J, Yang Y, Zhang W, Wang S (2019) Oxygen migration characteristics during bamboo torrefaction process based on the properties of torrefied solid, gaseous, and liquid products. Biomass Bioenergy 128:105300. https://doi.org/10.1016/j.biombioe.2019.105300

MacLeod M, Arp HPH, Tekman MB, Jahnke A (2021) The global threat from plastic pollution. Science 373:61–65. https://doi.org/10.1126/science.abg5433

MEPRC (Ministry of Environment of the People's Republic of China) (2020) Communiqué of the Second National Survey of Pollution Sources. https://www.mee.gov.cn/xxgk2018/xxgk/xxgk01/202006/W020200610353985963290. Accessed 2 Jan 2024

Mohseni-Bandpei A, Majlesi M, Rafiee M, Nojavan S, Nowrouz P, Zolfagharpour H (2019) Polycyclic aromatic hydrocarbons (PAHs) formation during the fast pyrolysis of hazardous health-care waste. Chemosphere 227:277–288. https://doi.org/10.1016/j.chemosphere.2019.04.028

Oh SY, Seo TC (2019) Upgrading biochar via co-pyrolyzation of agricultural biomass and polyethylene terephthalate wastes. RSC Adv 9(48):28284–28290. https://doi.org/10.1039/C9RA05518E

Park JH, Wang JJ, Kim SH, Kang SW, Jeong CY, Jeon JR, Park KH, Cho JS, Delaune RD, Seo DC (2019) Cadmium adsorption characteristics of biochars derived using various pine tree residues and pyrolysis temperatures. J Colloid Interface Sci 553:298–307. https://doi.org/10.1016/j.jcis.2019.06.032

Parikh SJ, Mukome FND, Zhang X (2014) ATR–FTIR spectroscopic evidence for biomolecular phosphorus and carboxyl groups facilitating bacterial

adhesion to iron oxides. Colloids Surf B 119:38–46. https://doi.org/10.1016/j.colsurfb.2014.04.022
Qi R, Jones DL, Li Z, Liu Q, Yan C (2020) Behavior of microplastics and plastic film residues in the soil environment: a critical review. Sci Total Environ 703:134722. https://doi.org/10.1016/j.scitotenv.2019.134722
Qin G, Niu Z, Yu J, Li Z, Ma J, Xiang P (2021) Soil heavy metal pollution and food safety in China: effects, sources and removing technology. Chemosphere 267:129205. https://doi.org/10.1016/j.chemosphere.2020.129205
Rathnayake D, Ehidiamhen PO, Egene CE, Stevens CV, Meers E, Mašek O, Ronsse F (2021) Investigation of biomass and agricultural plastic co-pyrolysis: effect on biochar yield and properties. J Anal Appl Pyrolysis 155:105029. https://doi.org/10.1016/j.jaap.2021.105029
Rodriguez JA, Lustosa Filho JF, Melo LCA, de Assis IR, de Oliveira TS (2021) Co-pyrolysis of agricultural and industrial wastes changes the composition and stability of biochars and can improve their agricultural and environmental benefits. J Anal Appl Pyrolysis 155:105036. https://doi.org/10.1016/j.jaap.2021.105036
Scarascia Mugnozza G, Schettini E, Loisi RV, Blanco I, Vox G (2016) Georeferencing of agricultural plastic waste. Rivista Di Studi Sulla Sostenibilita' 1:71–82. https://doi.org/10.3280/RISS2016-001007
Sebestyén Z, Barta-Rajnai E, Bozi J, Blazsó M, Jakab E, Miskolczi N, Sója J, Zs C (2017) Thermo-catalytic pyrolysis of biomass and plastic mixtures using HZSM-5. Appl Energy 207:114–122. https://doi.org/10.1016/j.apenergy.2017.06.032
Shen Z, Hou D, Jin F, Shi J, Fan X, Tsang DCW, Alessi DS (2019) Effect of production temperature on lead removal mechanisms by rice straw biochars. Sci Total Environ 655:751–758. https://doi.org/10.1016/j.scitotenv.2018.11.282
Shi W, Lian W, Tian S, Gong X, Yu Q, Guo Z, Zhang X, Ma B, Bian R, Zheng J, Cheng K, Pan G (2023) A review of agronomic and environmental properties of inorganic compounds in biochars. Curr Opin Env Sustain 5:100226. https://doi.org/10.1016/j.crsust.2023.100226
Sun T, Li Z, Zhang Z, Wang Z, Yang S, Yang Y, Wang X, Liu S, Zhang Q, Lei T (2020) Fast corn stalk pyrolysis and the influence of catalysts on product distribution. Bioresour Technol 301:122739. https://doi.org/10.1016/j.biortech.2020.122739
Tang KHD (2023) Microplastics in agricultural soils in China: Sources, impacts and solutions. Environ Pollut 322:121235. https://doi.org/10.1016/j.envpol.2023.121235
Wang C, Wang Y, Herath HMSK (2017) Polycyclic aromatic hydrocarbons (PAHs) in biochar – Their formation, occurrence and analysis: a review. Org Geochem 114:1–11. https://doi.org/10.1016/j.orggeochem.2017.09.001
Wang J, Xia K, Waigi M, Gao Y, Odinga E, Ling W, Liu J (2018a) Application of biochar to soils may result in plant contamination and human cancer risk due to exposure of polycyclic aromatic hydrocarbons. Environ Int 121:169–177. https://doi.org/10.1016/j.envint.2018.09.010
Wang L, Li C, Jiao B, Li Q, Su H, Wang J, Jin F (2018b) Halogenated and parent polycyclic aromatic hydrocarbons in vegetables: Levels, dietary intakes, and health risk assessments. Sci Total Environ 616:288–295. https://doi.org/10.1016/j.scitotenv.2017.10.336
Wang RZ, Huang DL, Liu YG, Zhang C, Lai C, Zeng GM, Cheng M, Gong XM, Wan J, Luo H (2018c) Investigating the adsorption behavior and the relative distribution of Cd2+ sorption mechanisms on biochars by different feedstock. Bioresour Technol 261:265–271. https://doi.org/10.1016/j.biortech.2018.04.032
Wang X, Zhao Y, Deng J, Zhou Y, Yuan S (2023) Study on the influence mechanism of mineral components in biochar on the adsorption of Cr(VI). Fuel 340:127631. https://doi.org/10.1016/j.fuel.2023.127631
Wang Z, Burra KG, Lei T, Gupta AK (2021) Co-pyrolysis of waste plastic and solid biomass for synergistic production of biofuels and chemicals-A review. Prog Energy Combust Sci 84:100899. https://doi.org/10.1016/j.pecs.2020.100899
Wu J, Wang T, Zhang Y, Pan WP (2019) The distribution of Pb(II)/Cd(II) adsorption mechanisms on biochars from aqueous solution: Considering the increased oxygen functional groups by HCl treatment. Bioresour Technol 291:121859. https://doi.org/10.1016/j.biortech.2019.121859
Wu M, Wang Z, Chen G, Zhang M, Sun T, Wang Q, Zhu H, Guo S, Chen Y, Zhu Y, Lei T, Burra KG, Gupta AK (2023) Synergistic effects and products distribution during Co-pyrolysis of biomass and plastics. J Energy Inst 111:101392. https://doi.org/10.1016/j.joei.2023.101392
Xie T, Yao Z, Huo L, Jia J, Zhang P, Tian L, Zhao L (2023) Characteristics of biochar derived from the co-pyrolysis of corn stalk and mulch film waste. Energy 262:125554. https://doi.org/10.1016/j.energy.2022.125554
Xu C, Zhang B, Gu C, Shen C, Yin S, Aamir M, Li F (2020) Are we underestimating the sources of microplastic pollution in terrestrial environment? J Hazard Mater 400:123228. https://doi.org/10.1016/j.jhazmat.2020.123228
Yan L, Liu Y, Zhang Y, Liu S, Wang C, Chen W, Liu C, Chen Z, Zhang Y (2020) $ZnCl_2$ modified biochar derived from aerobic granular sludge for developed microporosity and enhanced adsorption to tetracycline. Bioresour Technol 297:122381. https://doi.org/10.1016/j.biortech.2019.122381
Yang X, Ng W, Wong BSE, Baeg GH, Wang CH, Ok YS (2019) Characterization and ecotoxicological investigation of biochar produced via slow pyrolysis: Effect of feedstock composition and pyrolysis conditions. J Hazard Mater 365:178–185. https://doi.org/10.1016/j.jhazmat.2018.10.047
Yao A, Liu Y, Luo X, Liu C, Tang Y, Wang S, Huang X, Qiu R (2021) Mediation effects of different sulfur forms on solubility, uptake and accumulation of Cd in soil-paddy rice system induced by organic carbon and liming. Environ Pollut 279:116862. https://doi.org/10.1016/j.envpol.2021.116862
Yuan JH, Xu RK, Zhang H (2011) The forms of alkalis in the biochar produced from crop residues at different temperatures. Bioresour Technol 102:3488–3497. https://doi.org/10.1016/j.biortech.2010.11.018
Yuan S, Hong M, Li H, Ye Z, Gong H, Zhang J, Huang Q, Tan Z (2020) Contributions and mechanisms of components in modified biochar to adsorb cadmium in aqueous solution. Sci Total Environ 733:139320. https://doi.org/10.1016/j.scitotenv.2020.139320
Zhang B, Cui G, Jia W, Xia R, Lan Z, Wang Z, Jiang J, Yu Q, Dong S (2017) Soilless cultivation technology of small-fruited watermelon hanging vine in multi-story greenhouse. Chin Melon Veg 30:42–4. https://doi.org/10.16861/j.cnki.zggc.2017.0092
Zhang C, Nie S, Liang J, Zeng G, Wu H, Hua S, Liu J, Yuan Y, Xiao H, Deng L, Xiang H (2016) Effects of heavy metals and soil physicochemical properties on wetland soil microbial biomass and bacterial community structure. Sci Total Environ 557–558:785–790. https://doi.org/10.1016/j.scitotenv.2016.01.170
Zhang D, Ng EL, Hu W, Wang H, Galaviz P, Yang H, Sun W, Li C, Ma X, Fu B, Zhao P, Zhang F, Jin S, Zhou M, Du L, Peng C, Zhang X, Xu Z, Xi B, Liu X, Sun S, Cheng Z, Jiang L, Wang Y, Gong L, Kou C, Li Y, Ma Y, Huang D, Zhu J, Yao J, Lin C, Qin S, Zhou L, He B, Chen D, Li H, Zhai L, Lei Q, Wu S, Zhang Y, Pan J, Gu B, Liu H (2020) Plastic pollution in croplands threatens long-term food security. Global Change Biol 26:3356–3367. https://doi.org/10.1111/gcb.15043
Zhang J, Guo N, Ding W, Han B, Zhao M, Wang X, Wang J, Cao B, Zou G, Chen Y (2023) Microplastic pollution and the related ecological risks of organic composts from different raw materials. J Hazard Mater 458:131911. https://doi.org/10.1016/j.jhazmat.2023.131911
Zhang J, Liu J, Liu R (2015) Effects of pyrolysis temperature and heating time on biochar obtained from the pyrolysis of straw and lignosulfonate. Bioresour Technol 176:288–291. https://doi.org/10.1016/j.biortech.2014.11.011
Zhao L, Cao X, Wang Q, Yang F, Xu S (2013) Mineral constituents profile of biochar derived from diversified waste biomasses: implications for agricultural applications. J Environ Qual 42:545–552. https://doi.org/10.2134/jeq2012.0232
Zhou H, Wu C, Onwudili JA, Meng A, Zhang Y, Williams PT (2016) Influence of process conditions on the formation of 2–4 ring polycyclic aromatic hydrocarbons from the pyrolysis of polyvinyl chloride. Fuel Process Technol 144:299–304. https://doi.org/10.1016/j.fuproc.2016.01.013
Zhou X, Nolte MW, Mayes HB, Shanks BH, Broadbelt LJ (2014) Experimental and mechanistic modeling of fast pyrolysis of neat glucose-based carbohydrates. 1. Experiments and development of a detailed mechanistic model. Ind Eng Chem Res 53:13274–13289. https://doi.org/10.1021/ie502259w